Journal of Hazardous Materials 192 (2011) 476–484

Contents lists available at ScienceDirect

Journal of Hazardous Materials

journal homepage: www.elsevier.com/locate/jhazmat

Removal of reactive red-120 and 4-(2-pyridylazo) resorcinol from aqueous samples by Fe_3O_4 magnetic nanoparticles using ionic liquid as modifier

Ghodratollah Absalan[a,*], Mozaffar Asadi[a], Sedigheh Kamran[a], Leila Sheikhian[a,1], Douglas M. Goltz[b]

[a] Professor Masoumi Laboratory, Department of Chemistry, College of Science, Shiraz University, Hafeziyeh, Fars, 71454 Shiraz, Iran
[b] Department of Chemistry, University of Winnipeg, Winnipeg, MB, R3B 2E9 Canada

ARTICLE INFO

Article history:
Received 29 December 2010
Received in revised form 26 April 2011
Accepted 15 May 2011
Available online 20 May 2011

Keywords:
Magnetic nanoparticle
Ionic liquid
Adsorption
Azo dye

ABSTRACT

The nanoparticles of Fe_3O_4 as well as the binary nanoparticles of ionic liquid and Fe_3O_4 (IL-Fe_3O_4) were synthesized for removal of reactive red 120 (RR-120) and 4-(2-pyridylazo) resorcinol (PAR) as model azo dyes from aqueous solutions. The mean size and the surface morphology of the nanoparticles were characterized by TEM, DLS, XRD, FTIR and TGA techniques. Adsorption of RR-120 and PAR was studied in a batch reactor at different experimental conditions such as nanoparticle dosage, dye concentration, pH of the solution, ionic strength, and contact time. Experimental results indicated that the IL-Fe_3O_4 nanoparticles had removed more than 98% of both dyes under the optimum operational conditions of a dosage of 60 mg, a pH of 2.5, and a contact time of 2 min when initial dyes concentrations of 10–200 mg L^{-1} were used. The maximum adsorption capacity of IL-Fe_3O_4 was 166.67 and 49.26 mg g^{-1} for RR-120 and PAR, respectively. The isotherm experiments revealed that the Langmuir model attained better fits to the equilibrium data than the Freundlich model. The Langmuir adsorption constants were 5.99 and 3.62 L mg^{-1} for adsorptions of RR-120 and PAR, respectively. Both adsorption processes were endothermic and dyes could be desorbed from IL-Fe_3O_4 by using a mixed NaCl-acetone solution and adsorbent was reusable.

1. Introduction

Dye and dye stuffs are extensively used in various areas such as textile, plastic, food, cosmetic, carpet and paper industries [1–3]. Wastewaters of these industries contain dye with metals, salts, and other chemicals which may be toxic to aquatic environment. Charges of such wastes in water sources causes damage to ecological balance and affects photosynthetic activity [1]. Hence, the presence of dyes in wastewaters is a major environmental problem as they are generally resistant to degradation by biological treatment methods. Textile wastewater contaminated with azo reactive dyes needs to be treated by physical and chemical means before discharging. Azo dyes account for about 70% of dyes used in the textile industry, and since dyes are stable, recalcitrant, colorant, and even potentially carcinogenic and toxic, their release into the environment poses serious environmental, aesthetical and health problems [4]. Many investigations have been reported using different methods for the removal of dyes from water and wastewater including biological processes [5], combined chemical and biochemical processes [6], chemical oxidation [7], adsorption [8], coagulation, and membrane treatments [9]. A review of the literatures [5–9] indicates that the adsorption is one of the most applied techniques for dye removal. This is likely due to its simplicity and high level of effectiveness. In this regard, several types of natural and synthetic adsorbents have been evaluated for the removal of dyes from colored water and wastewater [2,10,11]. Among them, activated carbon is one of the most widely used adsorbents for environmental pollution control. The main disadvantage of activated carbon is its high cost of production and treatment [2,12]. Thus, many researchers have focused their efforts on optimizing adsorption and developing novel alternative adsorbents with high adsorptive capacity and low cost. To do this, much attention has recently been paid to nanotechnological techniques. Several articles have been published on the application of various nanoparticles for the treatment and remediation of pollutants in the environment [13–15], some even focusing specifically on dye removal [16–18]. For example, MgO nanoparticles were used for removal of reactive blue 19 and reactive red 198 from wastewater [4]. The adsorption ability of the chitosan nanoparticles was studied using anthraquinone type Acid Green 27 [16].

Nanomaterials have large specific surface areas, and thus a large fraction of active sites are available for appropriate chemical interaction. Surface modification of magnetic nanoparticles can be accomplished by physical/chemical adsorption of organic

* Corresponding author. Tel.: +98 711 6137206; fax: +98 711 2286008.
E-mail addresses: gubsulun@yahoo.com, absalan@susc.ac.ir (G. Absalan).
[1] Current address: Department of Chemistry, Islamic Azad University-Kazerun Branch, Kazerun, Iran.

0304-3894/$ – see front matter © 2011 Elsevier B.V. All rights reserved.
doi:10.1016/j.jhazmat.2011.05.046

compounds by four major techniques: organic vapor condensation, polymer coating, surfactant adsorption and direct silanation [19,20].

This paper focuses on the preparation of magnetic nanoparticles of Fe_3O_4 modified by ionic liquids (IL-Fe_3O_4) and characterization by electron microscopy (TEM), X-ray diffraction (XRD), dynamic light scattering (DLS), Fourier transform infrared (FTIR) spectroscopy and thermogravimetric analysis (TGA). Removal of reactive red 120 (RR-120) and 4-(2-pyridylazo) resorcinol (PAR), Table 1, were studied as model azo dyes with different functional groups.

The effects of different experimental conditions such as dosage of IL-Fe_3O_4 nanoparticle, concentrations of dyes, pH of the aqueous sample and contact times, on removal of both dyes were evaluated. Adsorption isotherms and thermodynamic parameters were characterized as well.

2. Experimental

2.1. Chemicals and reagents

Analytical grades of reactive red 120 and 4-(2-pyridylazo) resorcinol, sodium hydroxide solution (1.5 mol L^{-1}), hydrochloric acid (37%w/w), acetone, acetic acid (99.9%w/w), $FeCl_3{\cdot}6H_2O$ (96%w/w) and $FeSO_4{\cdot}7H_2O$ (99.9%w/w) were purchased from Merck. Stock solutions (1000 mg L^{-1}) of RR-120 and PAR were prepared. For treatment experiments, the dye solutions with concentrations in the range of 10–200 mg L^{-1} were prepared by successive dilution of the stock solution with distilled water. The pH adjustments were performed with HCl and NaOH solutions (0.01–1.0 mol L^{-1}). Ionic liquid, 1-hexyl-3-methylimidazolium bromide, [C_6MIM][Br] was prepared according to the procedure reported in the literature [21].

2.2. Apparatus

A UV–vis spectrophotometer equipped with a 1-cm quartz cell was used for recording the visible spectra and absorbance measurements. The XRD measurements were performed on the XRD Bruker D8 Advance. The FTIR spectra were recorded on a Shimadzu FTIR 8000 spectrometer. A transmission electron microscope (Philips CM 10 TEM) was used for recording of TEM images. TGA was done on the dried samples by a home-made TG analyzer.

A Metrohm 780 pH meter was used for monitoring the pH values. A water ultrasonicator (Model CD-4800, China) was used to disperse the nanoparticles in solution and a super magnet Nd–Fe–B (1.4 T, 10 cm × 5 cm × 2 cm) was used. All measurements were performed at ambient temperature.

2.3. Fabrication of ionic liquid modified magnetic nanoparticles

The nanoparticles of Fe_3O_4 were synthesized by mixing ferrous sulfate and ferric chloride in NaOH solution with constant stirring as recommended [22]. To obtain maximum yield for magnetic nanoparticles during co-precipitation process, the ideal molar ratio of Fe^{2+}/Fe^{3+} was about 0.5. The precipitates were heated at 80 °C for 30 min and were sonicated for 20 min, then washed three times with 50 mL of distilled water solution.

Modification of Fe_3O_4 nanoparticles was carried out using ionic liquid [C_6MIM][Br] under vigorous magnetic stirring for 30 min at 50 °C. The modified iron oxide nanoparticles (IL-Fe_3O_4) were collected by applying a magnetic field with an intensity of 1.4 T. The IL-Fe_3O_4 particles were washed three times with 50 mL distilled water. Nanoparticles and distilled water mixture was dispersed by ultrasonicator for 10 min at room temperature. Then, the IL-Fe_3O_4 nanoparticles were magnetically separated.

2.4. Dye removal experiments

Dye-removal ability of the synthesized IL-Fe_3O_4 was carried out by using batch technique for individual dye based on a procedure described as follows. Aliquots of 50 mL of the dye solutions with initial concentrations of 10–200 mg L^{-1} in the pH range of 3.0–12.0, adjusted by 0.l0 mol L^{-1} of HCl and NaOH solutions were prepared and transferred into individual beaker. A known dosage of IL-Fe_3O_4 in the range of 15–150 mg was added to each solution and the suspension was immediately stirred with a magnetic stirrer for a predefined period of time (1–20 min). After the mixing time elapsed, the IL-Fe_3O_4 nanoparticles were magnetically separated and the solution was analyzed for the residual dye. The percent adsorption of dye, i.e. the dye-removal efficiency of IL-Fe_3O_4, was determined by using the following equation:

$$\text{Dye removal efficiency (\%)} = \frac{C_0 - C_f}{C_0} \times 100$$

where C_0 and C_f represent the dye concentrations (mg L^{-1}) before and after adsorption, respectively. All tests were performed in duplicate at ambient temperature. The amount of suspension of IL-Fe_3O_4 nanoparticles after dye adsorption was magnetically separated and mother solution was spectrophotometrically analyzed for IL. The results revealed that no leaching of IL had occurred from the surface of nanoparticles.

2.5. Adsorption isotherms

The adsorption isotherm of a specific adsorbent represents its adsorptive characteristics which is very important for designing the adsorption processes [23]. Experiments for the estimation of the individual adsorption isotherms of RR-120 and PAR onto the IL-Fe_3O_4 surface were performed by adding various amounts of IL-Fe_3O_4, in the range of 15–150 mg, to a series of beakers containing 50 mL of 200 mg L^{-1} of the dye solution at pH 2.5. The solutions were stirred for 2 min at 25 °C to attain the equilibrium condition. The aqueous solutions were analyzed for the residual dye after applying the magnetic field for settlement of the nanoparticles. The amount of the dye adsorbed onto IL-Fe_3O_4 was calculated based on the following mass balanced equation:

$$q_e = \frac{V(C_0 - C_e)}{m}$$

where q_e (in mg g^{-1}) is the adsorption capacity (mg dye adsorbed onto gram amount of IL-Fe_3O_4), V is the volume of the dye solution (in L), C_0 and C_e are the initial and equilibrium dye concentrations (in mg L^{-1}), respectively; and m is the mass (in g) of dry IL-Fe_3O_4 added.

For evaluating the equilibrium adsorption, several isotherm models which are essential in designing and optimizing of adsorption processes [24,25], have been developed such as Langmuir [26], Freundlich [27], Redlich–Peterson [28], Dubinin–Radushkevich [29] and Temkin [30] models. The more common models used to investigate the adsorption isotherm are Langmuir and Freundlich.

The linearized form of the Langmuir isotherm [26], assuming monolayer adsorption on a homogeneous adsorbent surface, is expressed as:

$$\frac{C_e}{q_e} = \frac{1}{bq_{\max}} + \frac{C_e}{q_{\max}}$$

where $q_{\max}$ (mg g^{-1}) is the surface concentration at monolayer coverage and illustrates the maximum value of q_e that can be attained as C_e is increased. The b parameter is a coefficient related to the energy of adsorption and increases with increasing strength of the adsorption bond. Values of $q_{\max}$ and b are determined from the linear regression plot of (C_e/q_e) versus C_e.

Table 1
Some characteristics of the investigated dyes.

Characteristic	RR 120	PAR
Molecular formula	$C_{44}H_{24}C_{l2}N_{14}Na_6O_{20}S_6$	$C_{11}H_9N_3O_2$
Color index name	Reactive Red-120	4-(2-Pyridylazo) resorcinol
Molecular weight	1470 (g mol^{-1})	215.21(g mol^{-1})
Water solubility	70 (g L^{-1})	-
λ_{max}	530 (nm)	390 (nm)
Class	Diazo (–N=N– bond)	Diazo (–N=N– bond)
Chemical structure		

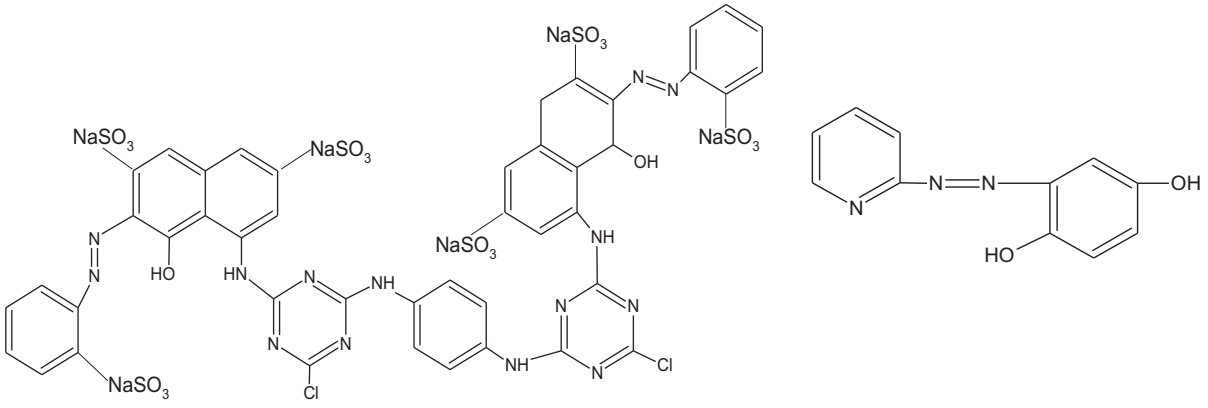

The Freundlich equation [27] is expressed in its linearized form as follows:

$$\log q_e = \log K_F + \frac{1}{n}\log C_e$$

where K_F and n are the constants from the Freundlich equation representing the capacity of the adsorbent for the adsorbate and the reaction order, respectively. The reciprocal reaction order, $1/n$, is a function of the strength of adsorption.

3. Results and discussion

3.1. Characterization of Fe_3O_4 and IL-Fe_3O_4

The peaks positions and relative intensities observed in XRD patterns of both IL-Fe_3O_4 nanoparticles and standard Fe_3O_4 are shown in Fig. 1 for comparison. Although the magnetic nanoparticle surfaces in IL-Fe_3O_4 were coated with ionic liquid, analysis of XRD patterns of both Fe_3O_4 and IL-Fe_3O_4 indicated very distinguishable peaks for magnetite crystal, which means that these particles have phase stability [31,32].

The FTIR spectra of Fe_3O_4, ionic liquid and IL-Fe_3O_4 are shown in Fig. 2. In the case of Fe_3O_4, the broad absorption band at 3440 cm^{-1} indicates the presence of surface hydroxyl groups (O–H stretching) and the bands at low wave numbers ($\leq$700 cm^{-1}) are related to vibrations of the Fe–O bonds in iron oxide. The presence of magnetite nanoparticles can be proven by appearance of two strong absorption bands around 632 and 585 cm^{-1} [33,34]. The Fe–O bond peak of the bulk magnetite is observed at 570.9 cm^{-1}. In the spectrum of ionic liquid (Fig. 2B), a longer hydrocarbon chain in [C_6MIM][Br] gives significantly stronger peaks in the ranges of 2800–3100 and 1465–1640 cm^{-1}. In the FTIR spectrum of IL-Fe_3O_4, the significant absorption band at 2923.9 cm^{-1} is due to the C–H stretching. The peak which is observed around 1180 cm^{-1}

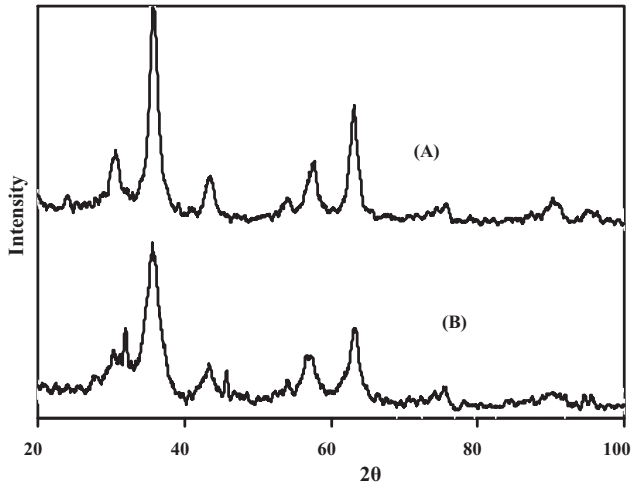

Fig. 1. XRD pattern of Fe_3O_4, A; and IL-Fe_3O_4, B.

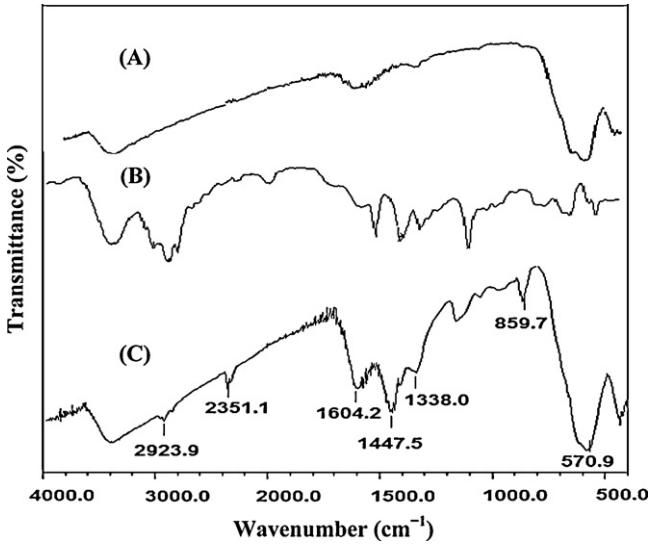

Fig. 2. FTIR spectra of Fe_3O_4, A; IL, B; and IL-Fe_3O_4, C.

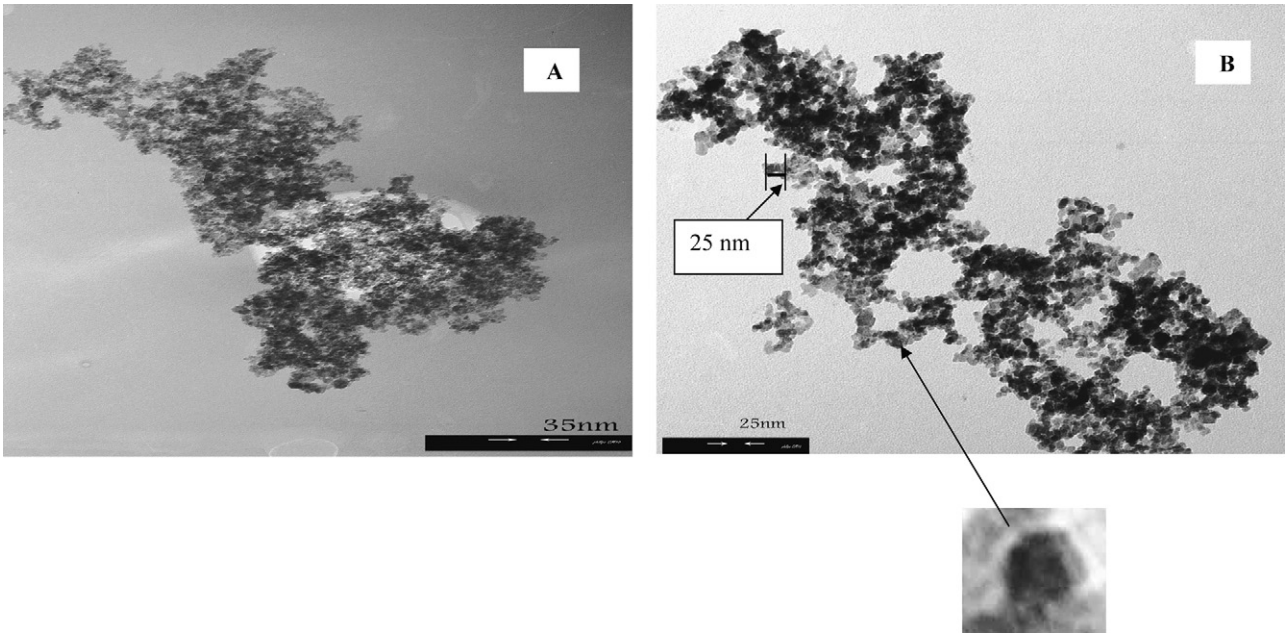

Fig. 3. The TEM image of Fe_3O_4, A; and IL-Fe_3O_4, B.

could be corresponding to the in plane C–H deformation vibration of imidazolium ring (Fig. 2B). The absorption band indicating the C–N stretching is observed at 1447.5 cm^{-1}. The absorption band at 1604 cm^{-1} is related to the hetero-aromatic C–H bond stretching.

Fig. 3 is a representative TEM image of Fe_3O_4 nanoparticles. The average diameter of Fe_3O_4 nanoparticles was about ~10 nm. However, the TEM image as shown in Fig. 3B indicated that IL-Fe_3O_4 (~13 nm) had a larger particle diameter than Fe_3O_4. If we assume that the difference of 3 nm in the mean sizes of both nanoparticles is significant then it revealed that ionic liquid caused agglomeration of Fe_3O_4 nanoparticles which was expected as ionic liquids could reduce the surface charges of nanoparticles which is a case similar to what can be observed for colloidal particles when an inert electrolyte is added to their aqueous solutions.

The magnetic nanoparticles were also characterized by dynamic light scattering [35], DLS (Fig. 4A and B). The DLS measures Brownian motion and relates this to the size of the particles. The size of a particle is calculated from the translational diffusion coefficient by using the Stokes–Einstein equation [35]:

$$D_t = \frac{TK_B}{3\pi\eta d}$$

In this equation: d = hydrodynamic diameter (in m), D_t = translational diffusion coefficient (in $m^2\ s^{-1}$), K_B = Boltzmann's constant, T = absolute temperature and η = viscosity (in $kg\ m^{-1}\ s^{-1}$). The diameter that is measured in DLS refers to how a particle diffuses within a fluid and is referred as a hydrodynamic diameter. The diameter that is obtained by this technique is the diameter of a sphere that has the same translational diffusion coefficient as the particle. The Fe_3O_4 and IL-Fe_3O_4 showed diameters of 80.8 and 82.3 nm, respectively.

The average particle diameters measured for the non-modified nanoparticles were much larger than those determined by TEM (~10 nm). The reason could be explained by the magneto static (magnetic dipole–dipole) interactions of the particles in the absence of any external magnetic field. This phenomenon was experimentally observed and confirmed by Monte Carlo simulations [36], i.e. formation of closed rings and long open loops of particles without preferential spatial orientation. The aggregates have a lower diffusion coefficient than single particles and the equivalent sphere radius measured by DLS is higher than the elementary particle size as revealed by TEM (Fig. 3A and B). In addition, the existence of a structured water layer adjacent to the hydrophilic surface of Fe_3O_4 can enhance the hydrodynamic radius measured by DLS as compared to TEM. For both nanoparticles (Fe_3O_4 and IL-Fe_3O_4) the diameter is smaller compared to that measured by DLS, presumably because TEM only shows the inorganic rich cores of the aggregates, i.e. the presence of the ionic liquid corona is not observed by TEM [37]. For both nanoparticles (Fe_3O_4 and IL-Fe_3O_4) the diameter is smaller compared to that measured by DLS, pre-

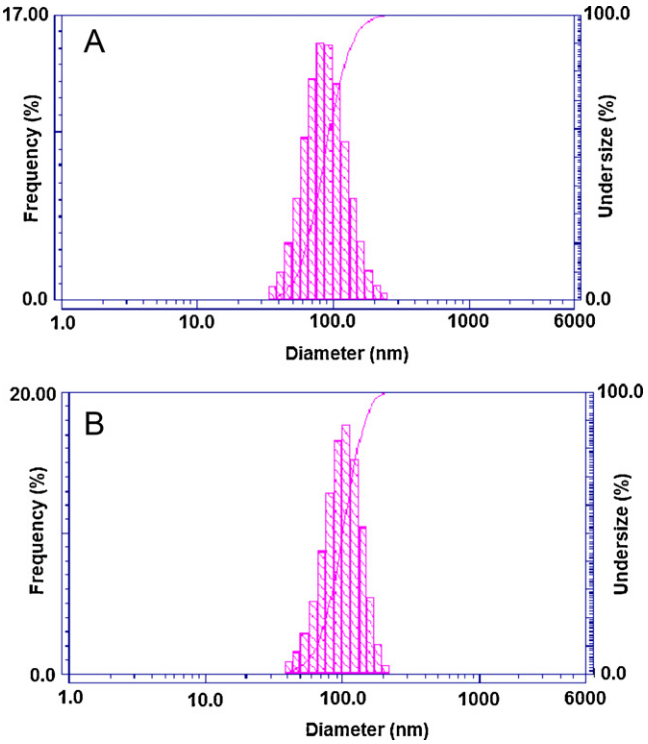

Fig. 4. Hydrodynamic diameter distributions of Fe_3O_4, A; and IL-Fe_3O_4, B.

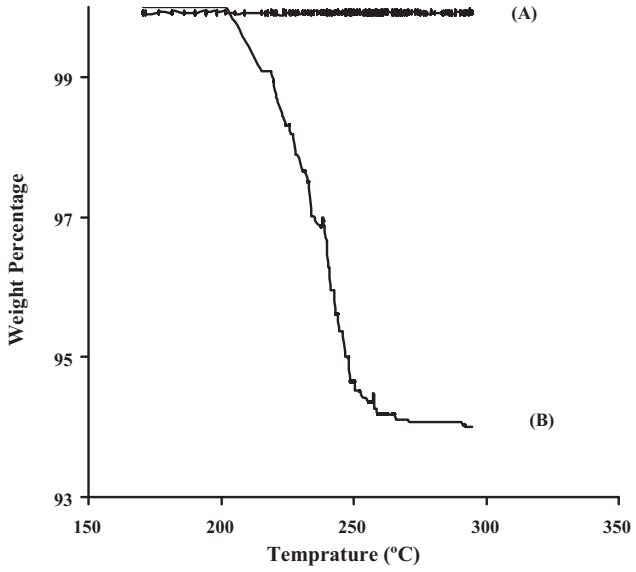

Fig. 5. TGA graphs of the Fe_3O_4, A; and IL-Fe_3O_4, B.

sumably because TEM only shows the inorganic rich cores of the Fe_3O_4 aggregates, i.e. the presence of the ionic liquid corona (in IL-Fe_3O_4 nanoparticles) or the structured water layer adjacent to the core in Fe_3O_4 nanoparticles are not observed by TEM [37].

To estimate the amount of ionic liquid deposited onto the surface of Fe_3O_4, the thermogravimetric analysis (TGA) of Fe_3O_4 and IL-Fe_3O_4 was conducted. Fig. 5 shows the TGA curves of both Fe_3O_4 and IL-Fe_3O_4 nanoparticles. In the lower temperature range (up to 201 °C), the initial weight loss was not observed. The weight loss of IL-Fe_3O_4 nanoparticles occurred in the temperature range of 201–261 °C was due to the decomposition of ionic liquid. At temperatures above 261 °C, the ionic liquid was completely decomposed. The residual weight should be the weight of Fe_3O_4. According to the TGA curves, the ionic liquid content of IL-Fe_3O_4 nanoparticles was evaluated to be 5.82% by weight.

The experimental curves corresponding to the immersion technique [38,39] were obtained for both sorbents and are presented in Fig. 6. Suspensions of 5.5 g L^{-1} of sorbents were prepared and individually were put into contact with 0.10 mol L^{-1} of NaCl solutions adjusted at different pH values. The aqueous suspensions were agitated for 48 h until the equilibrium pH was achieved. The pH value at the point of zero charge (pH_{pzc}) was determined by plotting the difference of final and initial pHs (ΔpH) versus the initial pH. As it is shown in Fig. 6, the pH_{pzc} values of both Fe_3O_4 and IL-Fe_3O_4 are 6.5 and 8.0, respectively, which means that the pH of Fe_3O_4 has shifted from 6.5 to 8.0 after modification with ionic liquid. This confirmed the deposition of ionic liquid onto the surface of Fe_3O_4 and also revealed that IL-Fe_3O_4 was positively charged at pH < 8.0.

3.2. Dye adsorption

The efficiencies of prepared Fe_3O_4 and IL-Fe_3O_4 as adsorbents for removal of RR-120 and PAR from aqueous solutions were investigated under different experimental conditions in order to find the optimum parameters as discussed below.

3.2.1. Effect of nanoparticle dosage

The effect of IL-Fe_3O_4 dosage on removal of RR-120 and PAR was investigated using a batch technique by adding a known quantity of the adsorbent, in the range of 15–150 mg of its powdered form, into individual beakers containing 50 mL of the dye solution. The resulting suspension was immediately stirred with a magnetic bar

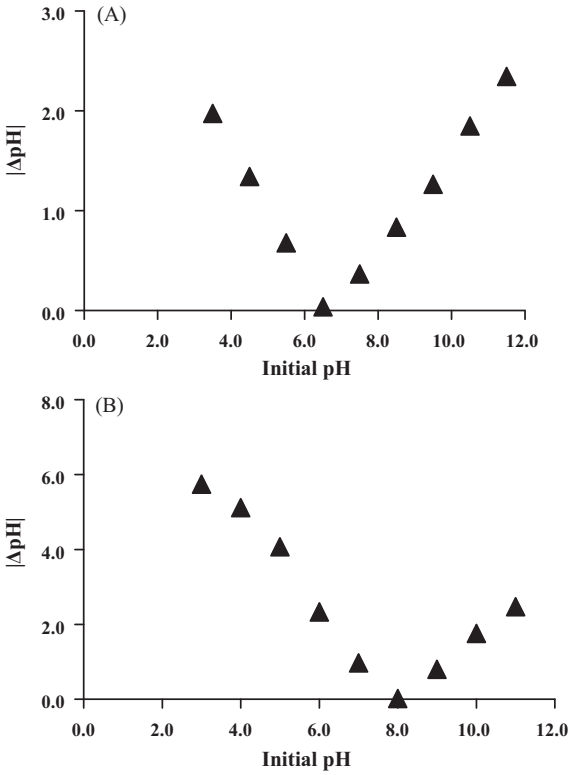

Fig. 6. Immersion technique curves of Fe_3O_4, A; and IL-Fe_3O_4, B.

for 5 min. After the mixing time elapsed, the IL-Fe_3O_4 nanoparticles were magnetically separated and the solution was analyzed for the residual dye. For all measurements, the initial dye concentrations and the pH of the solutions were fixed at 20 mg L^{-1} and 2.5, respectively. Results shown in Fig. 7 indicate that 95% of RR-120 and 99.6% of PAR were removed from their individual aqueous solutions when an initial dosage of 15 mg IL-Fe_3O_4 was used. The percent removal of both dyes increased with increasing IL-Fe_3O_4 up to the dosage of 60 mg and eventually reached to a value of 99.98% for each one. This observation can be explained by the greater number of adsorption sites made available for dye molecules at greater Fe_3O_4 dosages [40]. Further increase of the adsorbent dosage did not affect the removal of dyes. Hence, the optimum dosage of IL-Fe_3O_4 powder

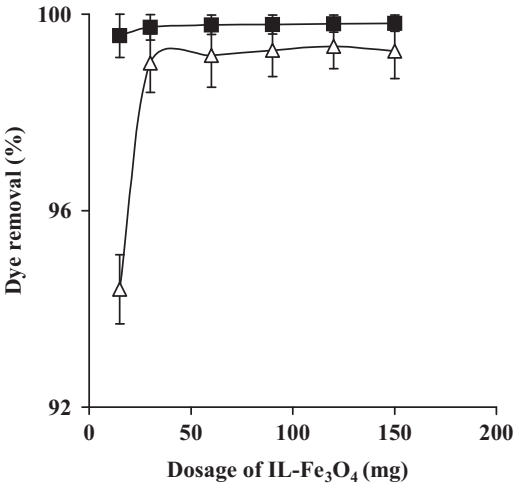

Fig. 7. Effect of initial dosage of IL-Fe_3O_4 nanoparticles on removal of RR-120 (△) and PAR (■). Experimental conditions: pH 2.0, initial dye concentration of 20 mg L^{-1}, stirring time of 5 min. The error bars correspond to percent average deviations.

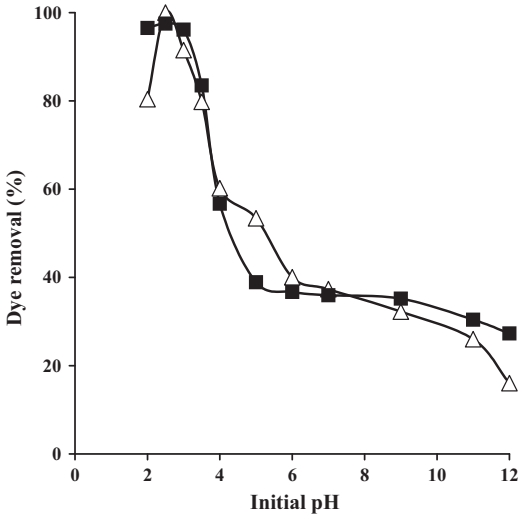

Fig. 8. Effect of initial pH of dye solution on removal of RR-120 (△) and PAR (■). Experimental conditions: IL-Fe_3O_4 dosage of 60 mg, initial dye concentration of 20 mg L^{-1}, stirring time of 5 min.

for removing both RR-120 and PAR from their individual solutions was found to be 60 mg.

3.2.2. Effect of solution pH

Solution pH is an important parameter that affects adsorption of dye molecules. The effect of the initial pH of the solution on the adsorption of RR-120 and PAR onto IL-Fe_3O_4 surfaces was assessed at different pH values, ranging from 1.0 to 12.0. The initial concentrations of both dyes and adsorbent dosage were set at 20 mg L^{-1} and 60 mg, respectively. The experiments were performed in a batch technique and each solution was stirred for 5 min. The results of this experiment are summarized in Fig. 8.

Fig. 8 shows that the initial pH of the sample solution could significantly affect the extent of adsorption of both dyes. Since the populations of negatively charged nanoparticles are expected to be increased by increasing pH, the percent removal of dyes is firstly increased as long as the dyes molecules are present in their positive or neutral forms which is the case in the pH values lower than ~2.0. It should be mentioned that at low pH values, the iron oxide nanoparticles dissolves as reported [41] and observed.

At pH more than 2.5, the anionic form of RR-120 predominates and an electrostatic repulsion is developed between both negatively charged nanoparticles and RR-120 molecules. The results of this experiment, shown in Fig. 8 indicate that there is a decrease in percent removal of dye as pH increases to values more than 2.5. It should be mentioned that the pK value for hydrolysis of the sulfonate groups of RR-120 is 2.1. For PAR with pKNH, pKOH (para), pKOH (ortho) values of 3.1, 5.6, 11.9, respectively, a similar decrease for its percent removal was observed at pH ~3.0 and higher due to the deprotonation of the –NH– group. At pH more than ~5.0 the percent removal of PAR was almost the same for all pH values as –OH (para) group dissociated and negatively charged PAR molecules produced. Generally, the higher adsorption of dyes at lower pH values could be due to the electrostatic attractions between negatively charged dyes anions and positively charged nanoparticles, whereas at higher pH values the abundance of OH^- are expected to prevent the adsorption of the anionic dye molecules [42]. Similar results were reported for the adsorption of other reactive dyes from aqueous solutions [43]. It should be mentioned that the value of pH_{pzc}, as explained in Section 3.1, revealed that the deposition of ionic liquid onto the surface of Fe_3O_4 produces IL-Fe_3O_4 with more positive charges at pH < 8.

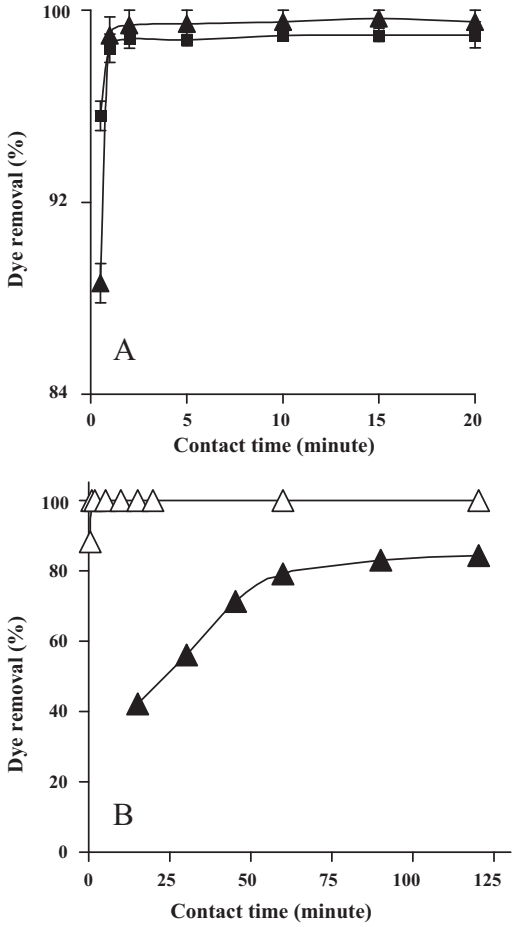

Fig. 9. (A) Effect of stirring time on removal of RR-120 (△) and PAR (■); (B) effect of stirring time on removal of RR-120 by Fe_3O_4 (▲) and IL-Fe_3O_4 (△). Experimental conditions: Fe_3O_4 and IL-Fe_3O_4 dosages of 60 mg, initial dyes concentrations of 20 mg L^{-1}, at pH 2.5. The error bars correspond to percent average deviations.

3.2.3. Effect of contact time

The contact time between adsorbate and adsorbent is one of the most important design parameters that affect the performance of adsorption processes. The effects of both contact and stirring time periods on the performance of IL-Fe_3O_4 for adsorbing RR-120 and PAR were investigated individually. The IL-Fe_3O_4 dosage of 60 mg and a solution pH of 2.5 were used for this investigation. The initial dye concentration for all test solutions were 20 mg L^{-1}. Fig. 9A shows removal efficiencies for both dyes as a function of stirring time ranging between 1 and 15 min. These data indicate that adsorption process started immediately upon adding the IL-Fe_3O_4 powder to both solutions. The removal efficiency for RR-120 rapidly increased from 88% ± 0.8% in the first minute of contact to a value of 99.4% ± 0.6%, where the equilibrium condition was attained, as the stirring was increased to 2 min. For PAR, the percentage of removal obtained in the first minute of stirring was 95.6% ± 0.6%, and complete removal was attained when the stirring was continued to 2 min. Thus, the contact time required to achieve equilibrium and complete adsorption for both of the tested model dyes was the same. Therefore, the optimum contact time between sample solution and IL-Fe_3O_4 nanoparticles was considered to be 2 min. The shorter the contact time in an adsorption system, the lower would be the capital and operational costs for real-world applications. The contact time obtained in this study was found to be shorter than most of the reported values for dyes adsorption by other adsorbents [25,33].

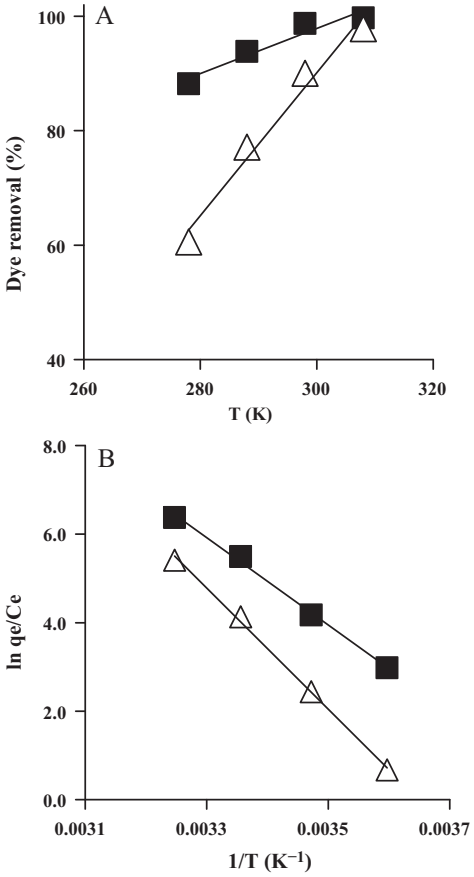

Fig. 10. (A) Effect of temperature on removal of RR-120 (△) and PAR (■); (B) the plots of $\ln(q_e/C_e)$ against $1/T$ for RR-120 (△) and PAR (■).

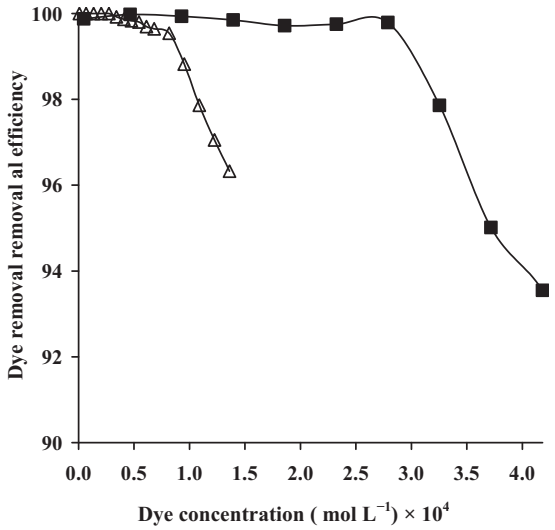

Fig. 11. Effect of initial dye concentration on removal of RR-120 (△) and PAR (■). Experimental conditions; IL-Fe_3O_4 dosage of 60 mg, pH 2.5, stirring time of 2 min.

It is noticeable that the adsorption of RR-120 onto the prepared Fe_3O_4 was studied first. Fig. 9B shows the comparison of adsorption of RR-120 onto Fe_3O_4 and IL-Fe_3O_4 nanoparticles. The results showed that a contact time of 90 min was required when unmodified nanoparticle was used. Considering Fig. 9B, the dye-removal efficiency by IL-Fe_3O_4 in comparison with Fe_3O_4 nanoparticles is higher. The presence of ionic liquid on the surface of nanoparticles increases both electrostatic and hydrophobic interactions between IL-Fe_3O_4 and dyes which consequently increases both rate of dye-adsorption process and dye-removal efficiency. This also shortens the contact time required for dyes to be quantitatively removed by IL-Fe_3O_4 when compared with Fe_3O_4 nanoparticles.

3.2.4. Effect of solution temperature

The effect of temperature on the adsorption of RR-120 and PAR by IL-Fe_3O_4 was investigated at pH 2.5 and initial dyes concentrations of 20 mg L^{-1} with a stirring time of 2 min. Fig. 10A shows removal efficiencies for both dyes as a function of temperature ranging between 278 and 308 K. The results indicate that the solution temperature strongly affected the adsorption efficiency of RR-120. For instance, the adsorption efficiency of RR-120 was 62.6% at 278 K, but it increases to 99.90% at 308 K, which indicates the endothermic nature of the adsorption process. However, in comparison with RR-120, the adsorption efficiency of PAR was from 88.19% to 99.71%, under a similar temperature range.

The plot of $\ln(q_e/C_e)$ versus $1/T$ was indicated in the inset of Fig. 10B. From the slope and intercept, the changes of enthalpy (ΔH) and entropy (ΔS) at 278–308 K could be determined, respectively. Table 2 shows thermodynamic parameters of adsorption for RR-120 and PAR onto IL-Fe_3O_4 nanoparticles. The free energy of the adsorption processes for both dyes onto IL-Fe_3O_4 at all temperatures was negative indicating the feasibility of the process and the spontaneous nature of the adsorption. The negative ΔG value increased with increased temperature, indicating that the spontaneity adsorption is proportional to the temperature. The positive value of ΔH indicates that adsorption processes for both dyes onto IL-Fe_3O_4 are endothermic. The positive value of ΔS indicates that the dye molecules have got lower order by being adsorbed onto the surface of IL-Fe_3O_4.

3.2.5. Effect of solution ionic strength

Since the presence of any ion could affect on the hydrophobic and electrostatic interaction between dyes and surface of IL-Fe_3O_4 as adsorbent, the effect of solution ionic strength on removal of RR-120 and PAR was investigated under optimum experimental conditions in batch technique. A selected concentration of KCl in the range of 0.10–0.80 mol L^{-1} was added to individual beakers containing 50 mL of the tested dye solution. The resulting suspension was immediately stirred with a magnetic stirrer for 2 min. After the mixing time elapsed, the IL-Fe_3O_4 nanoparticles were magnetically separated and the solution was analyzed for the residual dye. The adsorption capacities of IL-Fe_3O_4 for PAR and RR120 were not significantly affected with increasing KCl concentration this indicates that Cl^- ions do not compete with the negative charge groups of the dye molecules for adsorption onto IL-Fe_3O_4 surface.

3.2.6. Effect of dye concentration

The dye concentration is another important variable that can affect its adsorption process. This will determine the concentration range of dye that could be quantitatively removed, i.e. the concentration range for which the adsorption efficiency is high and independent of the initial concentration of dye. To show this, different initial concentrations of RR-120 and PAR dyes were removed by IL-Fe_3O_4 under the previously determined optimum experimental conditions. Fig. 11 shows removal efficiency versus initial molar concentrations of dyes. This indicates that IL-Fe_3O_4 nanoparticles have greater capacity for adsorption of PAR than RR-120. This is due to the lower molecular weight and size of PAR as compared to RR-120.

Table 2
Thermodynamic parameters (±average deviation) of dyes-adsorption process onto IL-Fe_3O_4 nanoparticles.

Dye	ΔS_0^T (J mol^{-1} K^{-1})	ΔH_0^T (kJ mol^{-1})	ΔG_0^T (kJ mol^{-1})			
			278 K	288 K	298 K	308 K
RR-120	414.6 ± 4.3	113.6 ± 1.0	−1.7 ± 0.2	−5.8 ± 0.2	−9.9 ± 0.0	−14.1 ± 0.2
PAR	319.7 ± 4.1	82.0 ± 4.2	−6.9 ± 0.0	−10.1 ± 0.2	−13.3 ± 0.3	−16.5 ± 0.4

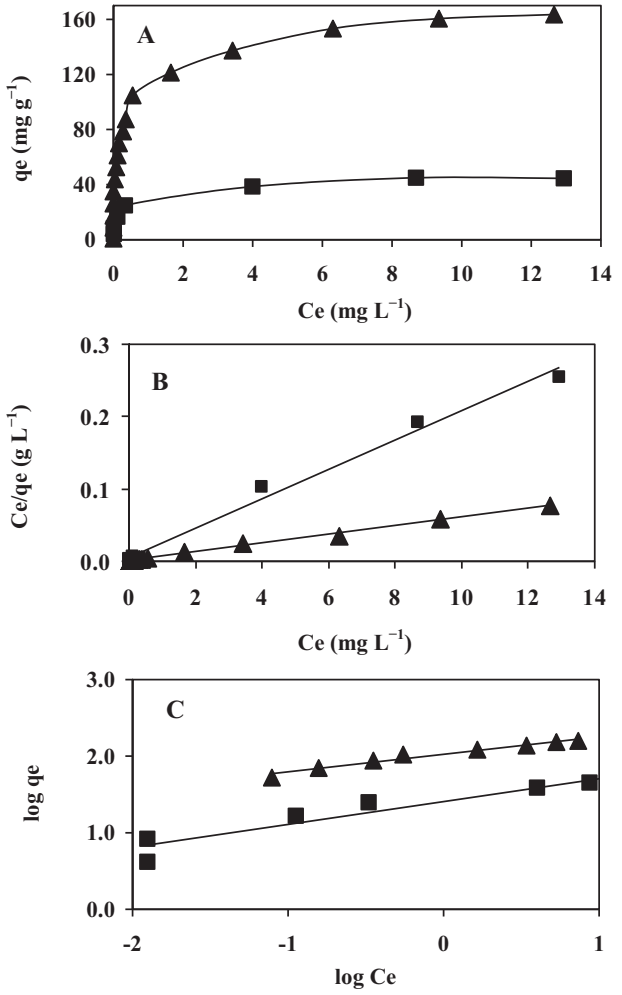

Fig. 12. (A) Equilibrium isotherms plots; (B) Langmuir isotherm plots; (C) Freundlich isotherm plots for RR-120 (▲) and PAR (■) adsorption onto IL-Fe_3O_4 nanoparticles. Experimental conditions: IL-Fe_3O_4 dosage of 15–150 mg, initial pH 2.5, stirring time of 2 min, initial dye concentration of 200 mg L^{-1}.

3.3. Adsorption isotherm modeling

The equilibrium adsorption data of RR-120 and PAR on IL-Fe_3O_4 surface were analyzed using Langmuir and Freundlich models. Model fits to equilibrium adsorption results of both dyes were assessed by the values of the determination coefficient (R^2) of the linear regression plot. The experimental data were fit with both models; the resulting plots are shown in Fig. 12A–C. Table 3 summarizes the models constants and the determination coefficients.

Table 3
Adsorption isotherms parameters of RR-120 and PAR onto IL-Fe_3O_4.

Dye	Langmuir model			Freundlich model		
	q_{max}	b	R^2	Log K_F	n	R^2
RR-120	166.67	3.62	0.9946	2.02	4.36	0.9663
PAR	49.26	5.99	0.9904	1.41	3.35	0.9084

As shown in Table 3, the R^2 of the Langmuir isotherm was greater than that of the Freundlich isotherm for the adsorption of both investigated dyes. This indicates that the adsorptions of RR-120 and PAR on IL-Fe_3O_4 nanoparticles are better described by the Langmuir model than the Freundlich model. This in turn suggests that adsorption occurs as the monolayer dyes adsorb onto the homogenous adsorbent surface. Table 3 shows that the maximum predictable adsorption capacity for RR-120 and PAR are 166.67 and 49.26 mg dye per gram IL-Fe_3O_4, respectively. It should be mentioned that the dye adsorption process is affected by the properties of both dyes and adsorbent as reported [44]. The difference in adsorption removal of RR-120 and PAR may be attributed to their chemical structures and physical properties, particularly the difference in the sizes of the dye molecules.

3.4. Desorption and reusability studies

For potential applications, the regeneration and reusability of an adsorbent are important factors to be reported. Possible desorption of RR-120 and PAR was tested by using different solutions such as mixed methanol/acetic acid solution (with different volume ratios of 1:1, 2:1 and 1:2), pure methanol, sodium chloride solution (1.0 mol L^{-1}) NaOH solution (1.0 mol L^{-1}), and mixed sodium chloride (1.0 mol L^{-1})/acetone (with volume ratios of 1:1, 2:1 and 1:2). The study revealed that the adsorbed RR-120 and PAR could be completely desorbed in the presence of mixed sodium chloride/acetone with a volume ratio of 2:1. In this study more than 98% of proposed dyes could be desorbed and recovered by 50 mL of sodium chloride (1 mol L^{-1})/acetone with a volume ratio of 2:1, when 1.0 mg dye (50 mL of dye with a concentration of 20 mg L^{-1}) was already adsorbed on IL-Fe_3O_4 nanoparticle. Addition of desorbing solution in multiple steps (3 steps as was obtained) can improved the desorption process as expected.

The reusability of the adsorbents in several successive separation processes was tested and the result showed that the IL-Fe_3O_4 nanoparticle can be recycled and reused for three times without significant reduction in its removal efficiency. The results also revealed that ionic liquid was stable for a period of 1 month at the surface of Fe_3O_4 showing that physical deposition of IL was probable.

4. Conclusions

A novel magnetic nano-adsorbent was fabricated by modifying the surface of Fe_3O_4 nanoparticles with [C_6MIM][Br] which was characterized by TEM, DLS, and XRD analysis. The FTIR analysis demonstrated the attachment of [C_6MIM][Br] on the surface of Fe_3O_4 nanoparticles was achieved via the interaction between the cationic part of [C_6MIM][Br] and the surface hydroxyl groups of Fe_3O_4. The results obtained by immersion technique confirmed the binding of ionic liquid on the surface of Fe_3O_4 nanoparticles and revealed the shift of the pH value at the point of zero charge (pH_{pzc}) from 6.5 to 8.0 after surface modification. With the help of TGA, the amount of [C_6MIM][Br] in the modified particles was determined to be about 5.82 wt% by weight. The IL-Fe_3O_4 nanoparticles were quite efficient as a magnetic nano-adsorbent for the fast removal of dyes from aqueous solutions. Magnetic nanoparticles have potential application in treatment of wastewater containing dyes. Short

contact time, high adsorption capacity, stability and reusability are advantages of IL-Fe_3O_4 nanoparticles as adsorbent.

The time required to achieve the adsorption equilibrium was 2 min. The adsorption of dyes on the surface of IL-Fe_3O_4 was concluded to be attributed to the electrostatic interaction between cationic part of IL and the ionic form of dyes, while the adsorption of dyes on the surface of Fe_3O_4 was mainly resulted due to interaction with surface hydroxyl groups of iron oxide. The adsorption data followed the Langmuir isotherm equation. The maximum adsorption capacities on IL-Fe_3O_4 and Langmuir adsorption constants were 166.67 mg g^{-1} and 5.99 L mg^{-1} for RR-120 and 49.26 m g g^{-1} and 3.62 L mg^{-1} for PAR, respectively. The changes of enthalpy (ΔH) were determined to be 113.6 and 81.99 kJ mol^{-1} for RR-120 and PAR, in the same order. In addition, NaCl-acetone solution was suitable for desorption of RR-120 and PAR and the reusability of IL-Fe_3O_4 was for three times.

Acknowledgments

The authors wish to acknowledge the support of this work by Shiraz University Research Council. We would like to thank DAJCO Company for generously supplying the magnet system, Dr. M. M. Doroodmand for TGA, Shiraz Nanotechnology Research Institute for DLS, Department of Physics for XRD and Veterinary Faculty for TEM.

References

[1] T. Robinson, G. Mcmullan, R. Marchant, P. Nigam, Remediation of dyes in textile effluent: a critical review on current treatment technologies with a proposed alternative, Bioresour. Technol. 77 (2001) 247–255.
[2] Z. Aksu, Application of biosorption for the removal of organic pollutants: a review, Process Biochem. 40 (2005) 997–1026.
[3] K. Vijayaraghavan, Y.S. Yun, Biosorption of C.I. reactive black 5 from aqueous solution using acid-treated biomass of brown seaweed Laminaria sp., Dyes Pigments 76 (2008) 726–732.
[4] G. Moussavi, M. Mahmoudi, Removal of azo and anthraquinone reactive dyes from industrial wastewaters using MgO nanoparticles, J. Hazard. Mater. 168 (2009) 806–812.
[5] M.Y. Arıca, G. Bayramo glu, Biosorption of reactive red-120 dye from aqueous solution by native and modified fungus biomass preparations of Lentinus sajorcaju, J. Hazard. Mater. 149 (2007) 499–507.
[6] L. Rizzo, J. Koch, V. Belgiorno, M.A. Anderson, Removal of methylene blue in a photocatalytic reactor using polymethylmethacrylate supported TiO_2 nanofilm, Desalination 211 (2007) 1–9.
[7] E. Kusvuran, O. Gulnaz, S. Irmak, O.M. Atanur, H.I. Yavuz, O. Erbatur, Comparison of several advanced oxidation processes for the decolorization of Reactive Red 120 azo dye in aqueous solution, J. Hazard. Mater. B109 (2004) 85–93.
[8] R. Han, D. Ding, Y. Xu, W. Zou, Y. Wang, Y. Li, L. Zou, Use of rice husk for the adsorption of congo red from aqueous solution in column mode, Bioresour. Technol. 99 (2008) 2938–2946.
[9] S. Papic, N. Koprivanac, A. Lonc, A. Metes, Removal of some reactive dyes from synthetic wastewater by combined Al (III) coagulation/carbon adsorption process, Dyes Pigments 62 (2004) 291–298.
[10] S. Karcher, A. Kornmuller, M. Jekel, Screening of commercial sorbents for the removal of reactive dyes, Dyes Pigments 51 (2001) 111–125.
[11] V.J.P. Vilar, C.M.S. Botelho, R.A.R. Boaventura, Methylene blue adsorption by algal biomass based materials: biosorbents characterization and process behavior, J. Hazard. Mater. 147 (2007) 120–132.
[12] M. Dias, M.C.M. Alvim-Ferraz, M.F. Almeida, J. Rivera-Utrilla, M. Snchez-Polo, Waste materials for activated carbon preparation and its use in aqueous-phase treatment: a review, J. Environ. Manage. 85 (2007) 833–846.
[13] B. Nagappa, G.T. Chandrappa, Mesoporous nanocrystalline magnesium oxide for environmental remediation, Micropor. Mesopor. Mater. 106 (2007) 212–218.
[14] B. Neppolian, Q. Wang, H. Jung, H. Choi, Ultrasonic-assisted sol–gel method of preparation of TiO_2 nano-particles: characterization, properties and 4-chlorophenol removal application, Ultrason. Sonochem. 15 (2008) 649–658.
[15] G. Zelmanov, R. Semiat, Iron (III) oxide-based nanoparticles as catalysts in advanced organic aqueous oxidation, Water Res. 42 (2008) 492–498.
[16] Z.G. Hu, J. Zhang, W.L. Chan, Y.S. Szeto, The sorption of acid dye onto chitosan nanoparticles, Polymer 47 (2006) 5838–5842.
[17] H.-Y. Shu, M.-C. Chang, H.-H. Yu, W.-H. Chen, Reduction of an azo dye Acid Black 24 solution using synthesized nanoscale zerovalent iron particles, J. Colloid Interface Sci. 314 (2007) 89–97.
[18] W.L. Du, Z.R. Xu, X.Y. Han, Y.L. Xu, Z.G. Miao, Preparation, characterization and adsorption properties of chitosan nanoparticles for eosin Y as a model anionic dye, J. Hazard. Mater. 153 (2008) 152–156.
[19] S.S. Banerjee, D.-H. Chen, Fast removal of copper ions by gum Arabic modified magnetic nano-adsorbent, J. Hazard. Mater. 147 (2007) 792–799.
[20] L. Bromberg, S. Raduyk, T.A. Hatton, Functional magnetic nanoparticles for biodefense and biological threat monitoring and surveillance, Anal. Chem. 81 (2009) 5637–5645.
[21] P. Bonhote, A.P. Dias, N. Papageorgion, K. Kalyanasundaran, M. Gratzel, Highly conductive ambient-temperature molten salts, Inorg. Chem. 35 (1996) 1168.
[22] D.K. Kim, Y. Zhang, W. Voit, K.V. Rao, M. Muhammed, Synthesis and characterization of surfactant-coated superparamagnetic monodispersed iron oxide nanoparticles, J. Magn. Magn. Mater. 225 (2001) 30–36.
[23] E. Erdem, G. Cölgeçen, R. Donat, The removal of textile dyes by diatomite earth, J. Colloid Interface Sci. 282 (2005) 314–319.
[24] R.D. Letterman, Water Quality and Treatment, 5th edition, McGraw-Hill, Inc., 1999.
[25] I.A.W. Tan, A.L. Ahmad, B.H. Hameed, Adsorption of basic dye on high-surface area activated carbon prepared from coconut husk: equilibrium, kinetic and thermodynamic studies, J. Hazard. Mater. 154 (2008) 337–346.
[26] I. Langmuir, The adsorption of gases on plane surfaces of glass, mica and platinum, J. Am. Chem. Soc. 40 (1918) 1361–1403.
[27] H.M.F. Freundlich, Over the adsorption in solution, J. Phys. Chem.-US 57 (1906) 385–471.
[28] O. Redlich, D.L. Peterson, A useful adsorption isotherm, J. Phys. Chem. 63 (1959) 1024–1026.
[29] T.P.O. Connor, J. Muller, Modeling competitive adsorption of chlorinated volatile organic compounds with the Dubinin–Radushkevich equation, Micropor. Mesopor. Mater. 46 (2001) 341–349.
[30] J.H. Chuna, S.K. Jeona, N.Y. Kima, J.Y. Chun, The phase-shift method for determining Langmuir and Temkin adsorption isotherms of over-potentially deposited hydrogen for the cathodic H2 evolution reaction at the poly-Pt/H_2SO_4 aqueous electrolyte interface, Int. J. Hydrogen Energy 30 (2005) 1423–1436.
[31] S.I. Park, J.H. Kim, J.H. Lim, C.O. Kim, Surface-modified magnetic nanoparticles with lecithin for applications in biomedicine, Curr. Appl. Phys. 8 (2008) 706–709.
[32] D. Faivre a, P. Zuddas, An integrated approach for determining the origin of magnetite nanoparticles, Earth Planet. Sci. Lett. 243 (2006) 53–60.
[33] R.D. Waldron, Infrared spectra of ferrites, Phys. Rev. 99 (1955) 1727.
[34] K. Can, M. Ozmen, M. Ersoz, Immobilization of albumin on aminosilane modified superparamagnetic magnetite nanoparticles and its characterization, Colloids Surf. B: Biointerfaces 71 (2009) 154–159.
[35] S. Chakraborty, B. Sahoo, I. Teraoka, R.A. Gross, Solution properties of starch nanoparticles in water and DMSO as studied by dynamic light scattering, Carbohydr. Polym. 60 (2005) 475–481.
[36] D. Maity, D.C. Agrawal, Synthesis of iron oxide nanoparticles under oxidizing environment and their stabilization in aqueous and non-aqueous media, J. Magn. Magn. Mater. 308 (2007) 46–55.
[37] A. Aqil a, S. Vasseur b, E. Duguet b, C. Passirani c, J.P. Benoît c, A. Roch d, R. Müller d, R. Jérôme a, C. Jérôme, PEO coated magnetic nanoparticles for biomedical application, Eur. Polym. J. 44 (2008) 3191–3199.
[38] N. Foil, I. Villaescusa, Determination of sorbent point zero charge: usefulness in sorption studies, Environ. Chem. Lett. 7 (2009) 79–84.
[39] M.T. Uddin, M.A. Islam, S. Mahmud, M. Rukanuzzaman, Adsorptive of removal of methylene blue by tea waste, J. Hazard. Mater. 164 (2009) 53–60.
[40] X. Wang, N. Zhu, B. Yin, Preparation of sludge-based activated carbon and its application in dye wastewater treatment, J. Hazard. Mater. 153 (2008) 22–27.
[41] B. Zargar, H. Parham, A. Hatamie, Modified iron oxide nanoparticles as solid phase extractor for spectrophotometric determination and separation of basic fuchsin, Talanta 77 (2009) 1328–1331.
[42] B.H. Hameed, A.A. Ahmad, N. Aziz, Isotherms, kinetics and thermodynamics of acid dye adsorption on activated palm ash, Chem. Eng. J. 133 (2007) 195–203.
[43] A. Özcan, A. Safa Özcan, Adsorption of Acid Red 57 from aqueous solutions onto surfactant-modified sepiolite, J. Hazard. Mater. B 125 (2005) 252–259.
[44] V. Rocher, J.-M. Siaugue, V. Cabuil, A. Bee, Removal of organic dyes by magnetic alginate beads, Water Res. 42 (2008) 1290–1298.